Cloud detection in the upper troposphere-lower stratosphere region via ACE imagers: A qualitative study

J. Dodion,[1] D. Fussen,[1] F. Vanhellemont,[1] C. Bingen,[1] N. Mateshvili,[1] K. Gilbert,[2] R. Skelton,[2] D. Turnbull,[2] S. D. McLeod,[2] C. D. Boone,[2] K. A. Walker,[2] and P. F. Bernath[2]

Received 3 February 2006; revised 9 September 2006; accepted 2 October 2006; published 9 February 2007.

[1] Satellite-based limb occultation measurements are well suited for the detection and mapping of polar stratospheric clouds (PSCs) and cirrus clouds. Usually, cloud signatures are detected on aerosol extinction profiles. In this paper, ACE two-dimensional (2-D) imager data are used to show PSCs and cirrus clouds. Clouds can be clearly seen, with a good vertical and horizontal resolution (1 km), during sunset and sunrise. In addition, we discovered significant differences between stratospheric (PSCs) and tropospheric (cirrus) clouds. PSCs appear as "symmetric" layers, no horizontal or vertical "structure" is detected within the PSC, suggesting that PSCs are uniform clouds with a very large horizontal extent. On the other hand, cirrus cloud image geometry is not well-defined. In contrast to PSCs, cirrus clouds appear as irregular shaped clouds. These tropospheric clouds seem to have horizontal dimensions similar to the Sun on the image (25 km at the tangent point). The qualitative display of these different kinds of clouds, seen on the raw 2-D imager data, proves the ability of the imagers to be an efficient cloud detector in the upper troposphere-lower stratosphere (UTLS) region. Moreover, the structure of these clouds can be derived.

Citation: Dodion, J., et al. (2007), Cloud detection in the upper troposphere-lower stratosphere region via ACE imagers: A qualitative study, *J. Geophys. Res.*, *112*, D03208, doi:10.1029/2006JD007160.

1. Introduction

[2] Polar stratospheric clouds are of fundamental importance for the formation of the Antarctic ozone hole [*Farman et al.*, 1985] that occurs every year since the early 1980s in Southern Hemisphere spring. PSCs act as hosts for heterogeneous reactions that transfer chlorine from the reservoir compounds HCl and $ClONO_2$ to Cl_2 [*Molina et al.*, 1987]. This process occurs throughout the polar night. When solar radiation reaches the polar lower stratosphere again, Cl_2 is photolyzed to active Cl that participates in a series of catalytic ozone destruction cycles [*Solomon*, 1999]. The formation of PSCs requires temperatures below 195 K (T_{NAT}) for PSC types Ia (NAT, nitric acid trihydrate; crystalline) and Ib (ternary solution of HNO_3, H_2SO_4 and H_2O; liquid), and less than about 188 K for PSC type II (H_2O ice).

[3] In addition, it has recently become clear that cirrus clouds significantly affect the global energy balance and climate, due to their influence on atmospheric thermal structure. Several studies [e.g., *Randall et al.*, 1989; *Ramaswamy and Ramanathan*, 1989; *Liu et al.*, 2003a; *Liu et al.*, 2003b] point out that cirrus clouds are likely to have great impact on the radiation and hence the intensity of the general large-scale circulation in the tropics. Cirrus are thin, wispy clouds that appear at high tropospheric altitudes and consist of ice crystals. Cirrus clouds are globally distributed at all latitudes over land or sea at any season of the year. They undergo continuous changes in area coverage, thickness, texture, and position. Tropical cirrus clouds extend as high as 13–18 km, with ice crystal sizes that range from about 10 to 2000 μm [*Eremenko et al.*, 2005].

[4] Distinguishing clouds from background aerosols in aerosol extinction retrievals is far from straightforward. The use of an averaged line of sight in retrieval methods for solar occultation measurements, the inhomogeneous nature of cloudiness, and the lack of coincident data available for comparisons make the distinction between clouds and aerosols very uncertain. Many approaches toward cloud identification from solar occultation and limb emission measurements have been attempted [e.g., *Kent et al.*, 1997; *Fromm et al.*, 1997; *Nedoluha et al.*, 2003; *von Savigny et al.*, 2005; *Spang et al.*, 2005]. Recently, the problem of PSC identification was also addressed using stellar occultation measurements [*Vanhellemont et al.*, 2005].

[5] In the present work, we used imager data provided by the Atmospheric Chemistry Experiment (ACE) to detect and illustrate cloud signatures. The main idea of our approach consists in first roughly detecting clouds using

[1]Belgian Institute for Space Aeronomy, Brussels, Belgium.
[2]Department of Chemistry, University of Waterloo, Waterloo, Ontario, Canada.

0148-0227/07/2006JD007160

transmission and total extinction profiles. A qualitative display of these different kinds of clouds, seen on the raw two-dimensional (2-D) imager data, will prove the ability of the imagers to be an efficient cloud detector in the upper troposphere-lower stratosphere (UTLS) region. Finally, a characteristic cloud image geometry for both PSCs and cirrus clouds is derived.

2. ACE Instrument and Imager Data

[6] The Atmospheric Chemistry Experiment (ACE) [*Bernath et al.*, 2005] was launched in August 2003 aboard the Canadian scientific satellite SCISAT-I. The main instrument on board is a high-resolution (0.02 cm^{-1}) Fourier Transform Spectrometer (FTS) operating from 750 to 4400 cm^{-1}. During sunrise and sunset, the FTS measures infrared absorption signals to provide (via an inversion) vertical profiles of atmospheric constituents (gases and particles). Aerosols and clouds are being monitored using the extinction of solar radiation at 1.02 (NIR) and 0.525 (VIS) μm as measured by two filtered imagers. The imagers consist of (after binning) 128 $\times$ 128 active pixel sensors. The total field of view (FOV) of the imagers is 30 mrad, to be compared to the 9 mrad angular diameter of the Sun. The signal-to-noise ratio (SNR) of each solar image is greater than 1000. The satellite operates from a circular orbit at an altitude of 650 km, and the orbital plane inclination of 74 degrees allows a global coverage with some predominance of the polar regions.

[7] While the Sun is setting below or rising from behind the Earth's horizon, at every time stamp, the imagers capture a snapshot of the Sun as seen through the atmosphere. On these pictures, the apparent Sun width is about 25 km at the tangent point and the apparent Sun height varies from almost 0.7 km (geometrical dimension of 1 pixel at the tangent point) in the optically thick, lower troposphere where the Sun image is highly flattened by the refraction, to its maximum (about 25 km at the tangent point) where refractive effects are negligible.

[8] Transmittances are calculated only for the pixels deemed to be in the center of the ACE-FTS FOV (i.e., the center of the Sun), as determined from the prelaunch registration measurements and postlaunch checks of the registration. The results are averaged for three adjacent pixels to improve the signal-to-noise ratio. The three pixels are within the FTS FOV and are from the same row of the image (and thus have the same tangent altitude). Tangent heights are assigned to the transmittance data through the time stamps of the ACE-FTS and imager measurements, with an accuracy of about 1 km. The authors refer to *Boone et al.* [2005] for a detailed description of ACE-FTS and imager retrievals. The imagers are sampled at a rate of 4 images per second, while the FTS scans take about 2 s each. The imagers and FTS are not synchronized to each other. So, an offset in time stamp is required to relate the two data sets. The value selected for the offset was chosen such that cloud features in the extinction profiles derived from the imagers matched observations from cloud spectral features in the FTS. From the transmittance data, a profile for total atmospheric extinction at both wavelengths was retrieved by using a vertical inversion algorithm.

[9] Aerosol extinction profiles were obtained by subtracting the gas extinction contributions (air, O_3, NO_2), obtained from the FTS measurements, from the total atmospheric extinction profiles. Since the used imager pixels are within the LOS of the FTS, our approach is reasonable. The temperature profiles that are used in this paper are also provided by the FTS.

3. Cloud Detection

[10] From the 3712 events measured between April 2004 and May 2005, we visually selected clouds from the imagers transmission and total extinction profiles. Clouds appear as sharp features, with a decrease in atmospheric transmittance corresponding to an increase in total extinction (Figure 1).

[11] The selected events are divisible in three main subgroups, determined by the three main ACE observation priorities (Arctic/Antarctic spring and the tropics). The first group of 38 clouds were visible during the (northern) winter of 2005 in Northern Hemisphere (>50°N). Second, we have a group of 59 clouds during the (northern) summer of 2004 in Southern Hemisphere (>50°S). Finally, there is a large group of 103 equatorial clouds (30°S to 30°N) in any season of the year 2004–2005. A longitude/latitude plot and a time/latitude plot shows the geographical and temporal distribution of the selected events (Figure 2).

[12] The median aerosol extinction profiles (Figure 3) clearly show an increased extinction in the lower stratosphere for the selected Southern Hemisphere occultations, revealing the presence of PSCs. At northern latitudes, no such stratospheric PSC signature is observed. This observation is corroborated by an investigation of the ACE temperature retrievals (Figure 4). In the majority of cases, temperatures exceed the PSC formation temperature (T_{NAT}). However, a few cases occur below T_{NAT} and these are associated with PSC formation. Other clouds are tropospheric clouds (increased upper tropospheric median aerosol extinction). At the equator, a significant median enhancement of aerosol extinction is observed below 17 km, suggesting the presence of tropospheric (cirrus) clouds.

4. Imager Results

[13] In this section we present a qualitative description of PSCs and cirrus clouds as seen by the NIR imager. The reason for not using the VIS imager is clear: optical extinction (gas absorption and Rayleigh scattering) is much stronger in the visible range. As a consequence, a signal cutoff is often observed at tropospheric and lower stratospheric altitudes. Moreover, transmittances that are measured by the NIR imager are almost exclusively affected by aerosols and clouds since the extinction cross sections of the gaseous species are very small at the corresponding wavelength.

[14] Starting from the set of detected cloud events, we have performed a classification. A cloud is labeled as a "PSC" when (1) the associated occultation occurred at high latitudes (possibly inside the polar vortex) and (2) when the associated temperature is lower than T_{NAT}. When at least one of these two criteria is not satisfied, the cloud is labeled as "cirrus." As already mentioned, many Northern Hemi-

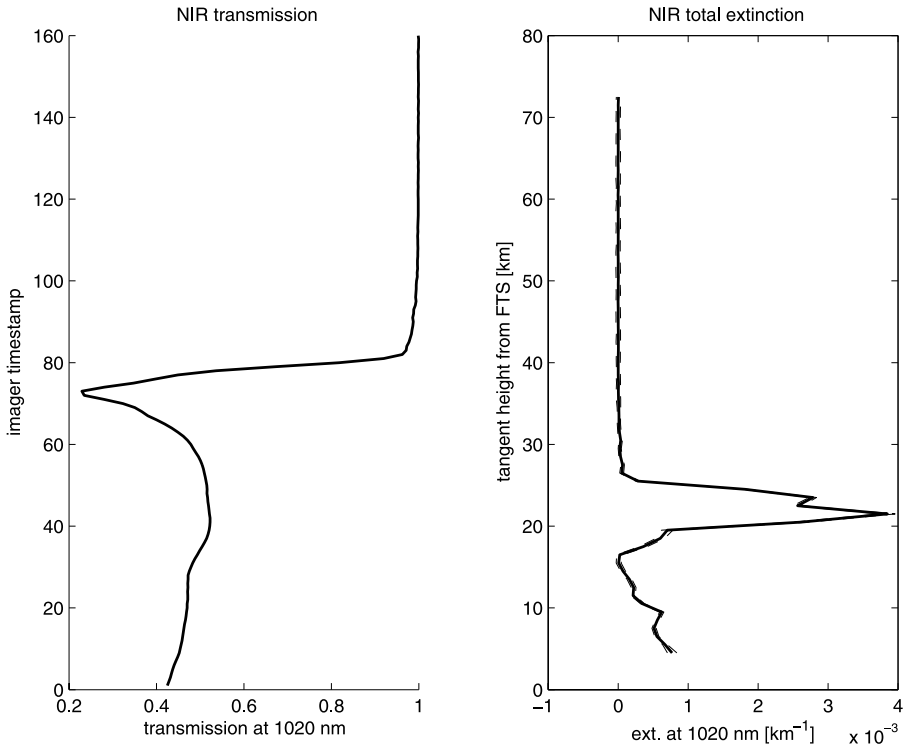

Figure 1. Atmospheric transmission (left) and total extinction (right) profile of a selected event with cloud contamination.

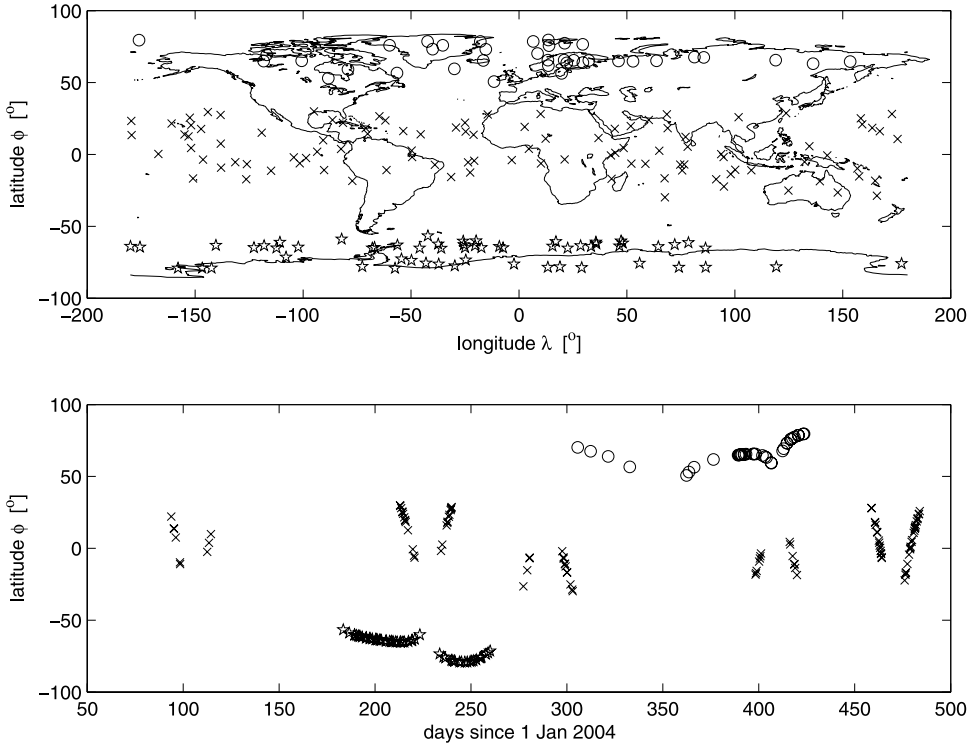

Figure 2. Geolocation of the selected events with possible cloud contamination at Northern Hemisphere (circles), equator (crosses) and Southern Hemisphere (stars). (top) Longitude/latitude plot; (bottom) time/latitude plot.

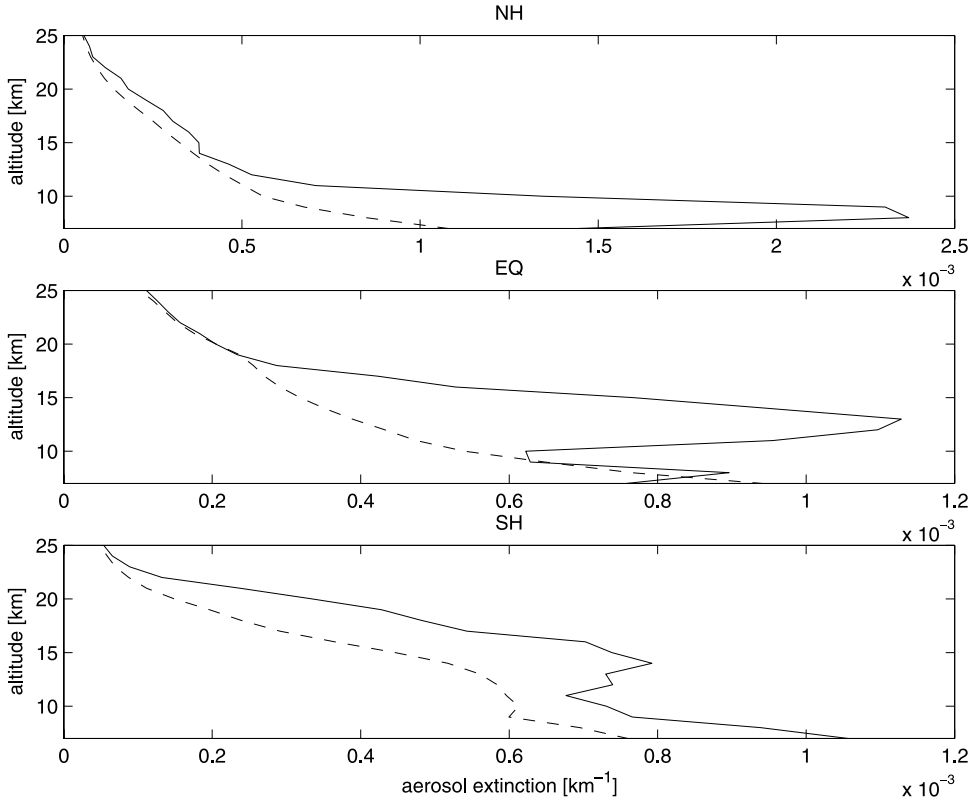

Figure 3. Median NIR aerosol extinction profiles for the selected events (full lines) in (top) Northern Hemisphere, (middle) equator, and (bottom) Southern Hemisphere. Dashed lines represent median NIR aerosol extinction profiles for events without cloud contamination.

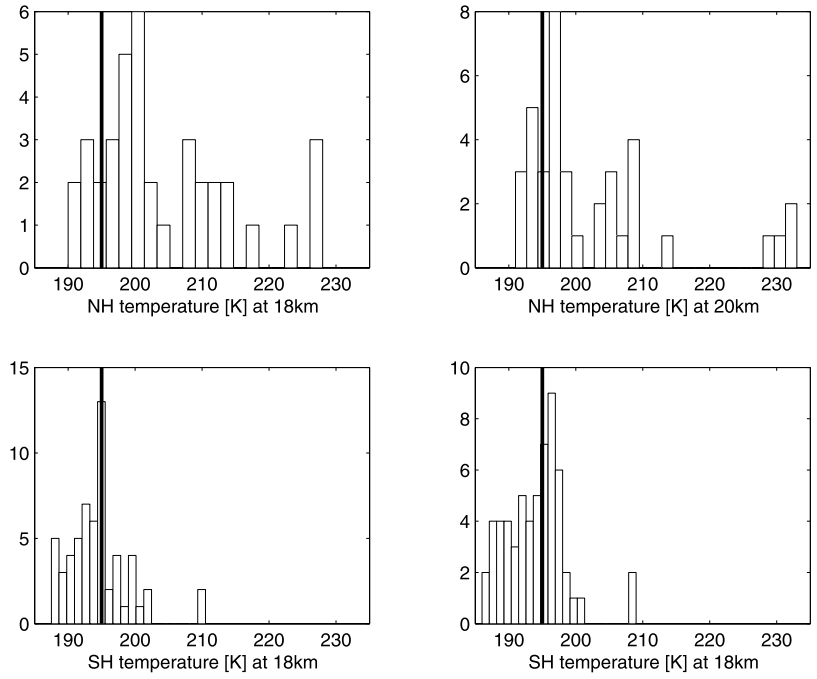

Figure 4. Temperature distributions for the selected occultations in (top) Northern Hemisphere and (bottom) Southern Hemisphere. T_{NAT} is indicated by the vertical line at 195 K.

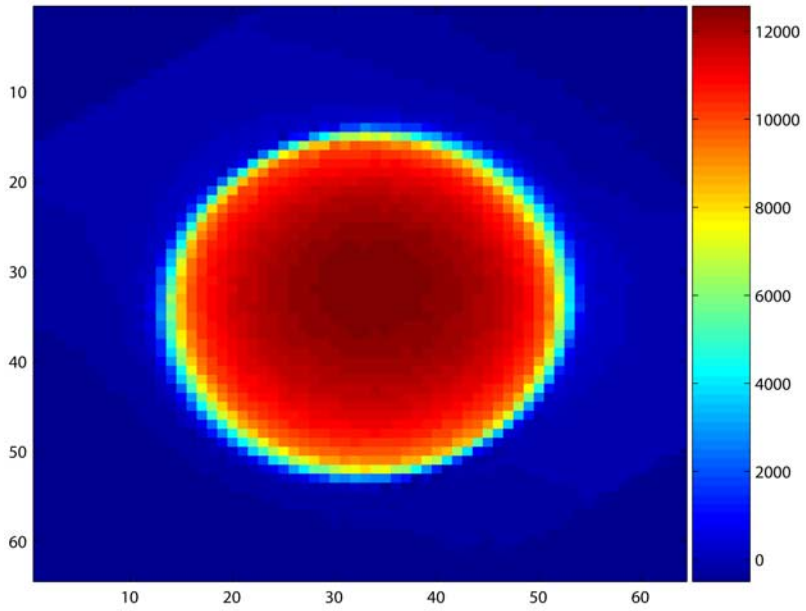

Figure 5. Reference Sun image outside the Earth's atmosphere (120 km). Note that vertical and horizontal scale is pixels (1 pixel has horizontal and vertical dimension of 0.7 km at the tangent point). The color bar represents measured flux intensity.

sphere clouds are suspected to be of the cirrus type. As we will see, the imager data confirm this beyond doubt.

[15] The images shown in this section are (raw) imager data. A rotation is applied to measured images such that the rows of the transformed image are parallel to the Earth's horizon. The transformation uses the assumed orientation of the satellite for aligning the input slit to the horizon (accurate to 1 degree). The images are corrected for items such as dark counts and secondary images. Presented images are one snapshot of the Sun, initially consisting of 64 $\times$ 64 pixels but cut off for distinct presentation. On Figure 5, an image of the Sun at high altitude, outside the Earth's atmosphere, is shown. Since there is no atmospheric

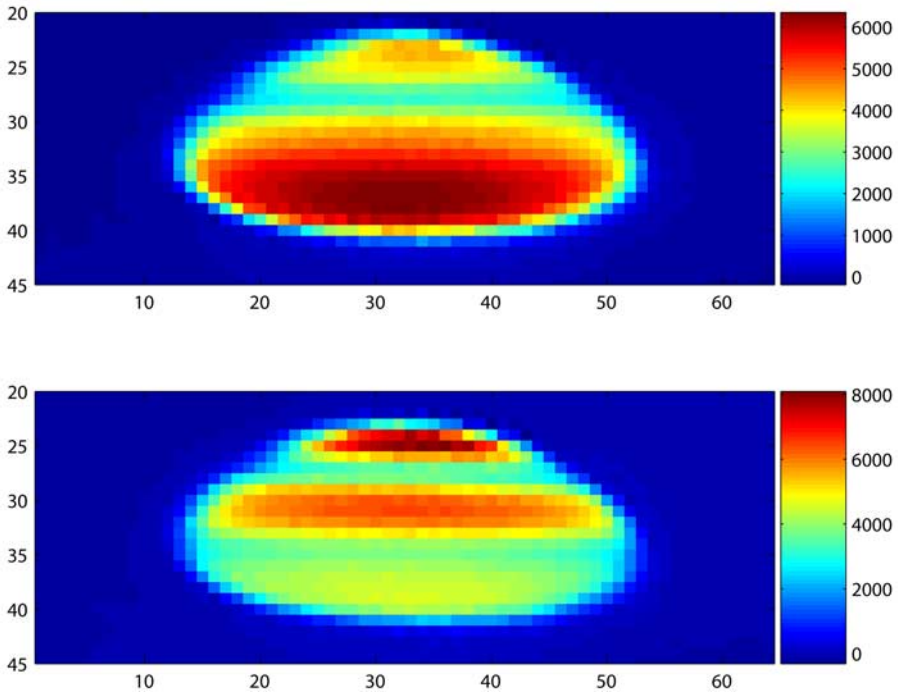

Figure 6. Imager data at 1.020 μm. (top) PSC layer, 9 July 2004 at lat = 61°S; (bottom) PSC double layer, 2 August 2004 at lat = 65°S.

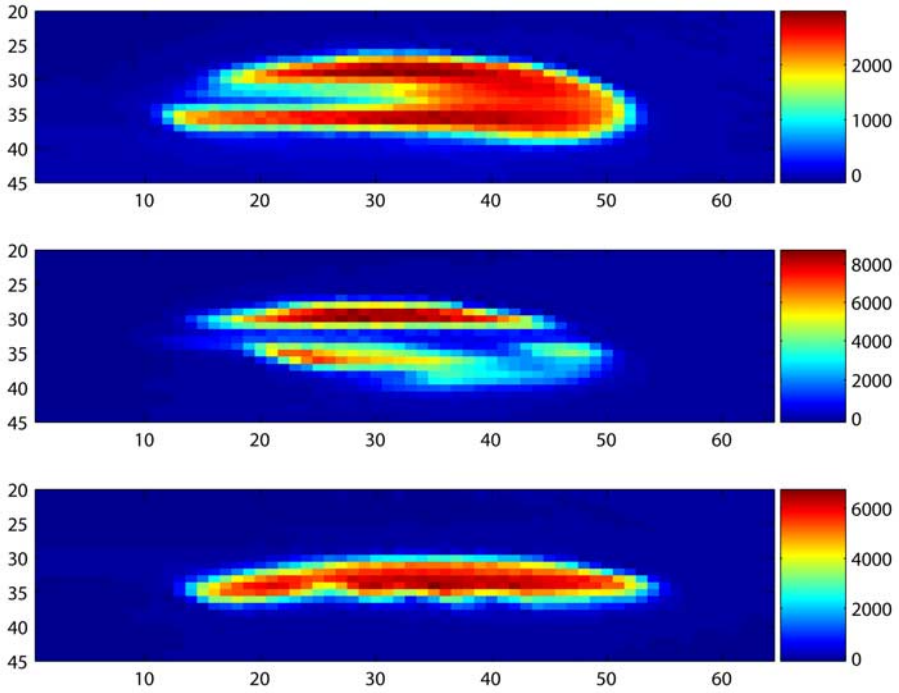

Figure 7. (top) Edge of a cirrus cloud, 20 February 2005 at lat = 5°N; (middle) cirrus cloud with complex structure, 26 August 2004, lat = 20°N; (bottom) cirrus cloud associated to cumulus structure, 27 August 2004, lat = 18°N

absorption, it is a reference image for other imager data in this section.

4.1. PSCs

[16] Imager data associated with PSC events, are shown on Figure 6. Remarkably, PSCs appear as "symmetric" layers. No horizontal or vertical "structure" is detected within the PSC, suggesting that PSCs are uniform clouds with a large horizontal extent. Owing to the good vertical resolution, even two PSCs above each other can be seen (a double layer). Looking to the movie of a Sun rising from behind the Earth's atmosphere, suddenly, between 15 and 25 km, a PSC appears on top of the Sun image. While the Sun is rising (setting), the cloud passes as a layer sliding down (up) over the solar disk. We detected no events with a PSC covering only a part of the Sun width. PSCs seem to be spread over very large, low-temperature, horizontal regions.

[17] In principle, cloud thickness should be derivable from imager data. However, it is important to notice that the cloud picture is dependent on the position of the cloud along the LOS. When the cloud is located near the tangent point, the cloud image geometry is a good indicator of the physical geometry. However, clouds located far from the tangent point region should be no exception. This is suggested by a significant amount of detected PSCs with a large altitude extent (10 km), most possibly caused by an altitude smearing.

4.2. Cirrus Clouds

[18] In contrast to PSCs, cirrus clouds are not characterized by a homogeneity in the imager data. Looking to the rising/setting Sun, cirrus clouds appear as horizontally and vertically moving, complex structures. This horizontal motion is not related to a physical motion of the cloud, but to β, i.e., the angle between the orbit track of the satellite and the Earth-Sun vector. The greater the absolute value of β, the faster the apparent horizontal movement of the cirrus cloud (the Sun is fixed in the CCD center).

[19] Obviously, there is a large variability in horizontal extent. However, edges are almost always detected. In contrast with PSCs, cirrus clouds seem to have horizontal dimensions similar to the Sun on the image (25 km at the tangent point). Single clouds are detected as well as groups of cirrus clouds. Also, cirrus clouds growing from outflows of tower cumuli in the tropics can be distinguished. Typically, these clouds absorb sunlight in the troposphere, forming a large chain of connected cirrus clouds (Figure 7). The conclusions for PSCs about the relation between observed cloud geometry and cloud location are of course also valid here.

4.3. Northern Hemisphere Observations

[20] When associated temperatures significantly exceed T_{NAT}, no PSC is observed. After further investigation of the ACE FTS temperature profiles, these clouds seem to be tropospheric (cirrus) clouds. These conclusions from section 3 remain unaffected after exploring 2-D imager data of the concerned events. Both horizontal extent as well as complexity of cloud structure support the subdivision of the Northern Hemisphere data set in PSCs and cirrus clouds. Using cloud image geometry, we obtain the same classification as via temperature investigation.

5. Conclusions

[21] ACE imager data are used to illustrate different types of clouds in the UTLS. A cloud is labeled as a "PSC" when the associated occultation occurred at high latitudes (possibly

inside the polar vortex) and when the associated temperature is lower than T_{NAT}. Otherwise, the cloud is labeled "cirrus cloud." We discovered significant differences between PSCs and cirrus clouds exploring 2-D imager data. PSCs appear as "symmetric" layers, no horizontal or vertical "structure" is detected within the PSC, suggesting that PSCs are uniform clouds with a very large horizontal extent. On the other hand, cirrus cloud image geometry is not well-defined. Also, cirrus clouds seem to have horizontal dimensions similar to the Sun on the image (25 km at the tangent point).

[22] In conclusion, we have established the usefulness of imager data to detect clouds and to observe their structure. Our conclusions about cloud image geometry will help us to implement a cloud detection algorithm in future. After validation, a synergetic use of ACE FTS and imager data will reveal observed cloud nature and geometry in the UTLS region. A (quantitative) cloud analysis at the tropics and at high latitudes during the polar vortices will be presented soon.

[23] **Acknowledgments.** The present study was funded by the PRODEX 7 contract SADE under the authority of the Belgian Space Science Office (BELSPO). The ACE mission is funded by the Canadian Space Agency and the Natural Sciences and Engineering Research Council of Canada (NSERC). Funding at Waterloo is also provided by the NSERC-Bomem-CSA-MSC Industrial Research Chair in Fourier Transform Spectroscopy.

References

Bernath, P. F., et al. (2005), Atmospheric Chemistry Experiment (ACE): Mission overview, *Geophys. Res. Lett.*, *32*, L15S01, doi:10.1029/2005GL022386.

Boone, C. D., R. Nassar, K. A. Walker, Y. Rochon, S. D. McLeod, C. P. Rinsland, and P. F. Bernath (2005), Retrievals for the atmospheric chemistry experiment Fourier-transform spectrometer, *Appl. Opt.*, *44*(33), 7218–7231.

Eremenko, M. N., A. Y. Zasetsky, C. D. Boone, and J. J. Sloan (2005), Properties of high-altitude tropical cirrus clouds determined from ACE FTS observations, *Geophys. Res. Lett.*, 32, L15S07, doi:10.1029/2005GL022428.

Farman, J. C., B. G. Gardiner, and J. D. Shanklin (1985), Large losses of total ozone in Antarctica reveal seasonal ClO_x/NO_x interaction, *Nature*, *315*, 207–210.

Fromm, M. D., R. M. Bevilacqua, J. D. Lumpe, E. P. Shettle, J. S. Hornstein, S. T. Massie, and K.-H. Fricke (1997), Observations of Antarctic polar stratospheric clouds by POAM II: 1994–1996, *J. Geophys. Res.*, *102*(D19), 23,659–23,672.

Kent, G. S., P.-H. Wang, and K. M. Skeens (1997), Discrimination of cloud and aerosol in the Stratospheric Aerosol and Gas Experiment III occultation data, *Appl. Opt.*, *36*(33), 8639–8649.

Liu, H.-L., P. K. Wang, and R. E. Schlesinger (2003a), A numerical study of cirrus clouds. Part I: Model description, *J. Atmos. Sci.*, *60*(8), 1075–1084.

Liu, H.-L., P. K. Wang, and R. E. Schlesinger (2003b), A numerical study of cirrus clouds. Part II: Effects of ambient temperature, stability, radiation, ice microphysics, and microdynamics on cirrus evolution, *J. Atmos. Sci.*, *60*(9), 1097–1119.

Molina, M. J., T. L. Tso, L. T. Molina, and F. C.-Y. Wang (1987), Antarctic stratospheric chemistry of chlorine nitrate, hydrogen chloride and ice: Release of active chlorine, *Science*, *238*, 1253–1257.

Nedoluha, G. E., R. M. Bevilaqua, M. D. Fromm, K. W. Hoppel, and D. R. Allen (2003), POAM measurements of PSCs and water vapor in the 2002 Antarctic vortex, *Geophys. Res. Lett.*, *30*(15), 1796, doi:10.1029/2003GL017577.

Ramaswamy, V., and V. Ramanathan (1989), Solar absorption of cirrus clouds and the maintenance of the tropical upper troposphere thermal structure, *J. Atmos. Sci.*, *46*, 2293–2310.

Randall, D. A., Harshovardan, D. A. Dazlich, and T. G. Corsetti (1989), Interactions among radiation, convection, and large-scale dynamics in a general circulation model, *J. Atmos. Sci.*, *46*, 1943–1970.

Solomon, S. (1999), Stratospheric ozone depletion: A review of concepts and history, *Rev. Geophys.*, *37*, 275–316.

Spang, R., J. J. Remedios, L. J. Kramer, L. R. Poole, M. D. Fromm, M. Müller, G. Baumgarten, and P. Konopka (2005), Polar stratospheric cloud observations by MIPAS on ENVISAT: Detection method, validation and analysis of the northern hemisphere winter 2002–2003, *Atmos. Chem. Phys.*, *5*, 392–679.

Vanhellemont, F., et al. (2005), A 2003 stratospheric aerosol extinction and PSC climatology from GOMOS measurements on Envisat, *Atmos. Chem. Phys.*, *5*, 2413–2417.

von Savigny, C., E. P. Ulasi, K.-U. Eichmann, H. Bovensmann, and J. P. Burrows (2005), Detection and mapping of polar stratospheric clouds using limb scattering observations, *Atmos. Chem. Phys.*, *5*, 3071–3079.

P. F. Bernath, C. D. Boone, K. Gilbert, S. D. McLeod, R. Skelton, D. Turnbull, and K. A. Walker, Department of Chemistry, University of Waterloo, 200 University Avenue W, Waterloo, Ontario, Canada N2L 3G1.

C. Bingen, J. Dodion, D. Fussen, N. Mateshvili, and F. Vanhellemont, Belgisch Instituut voor Ruimte-Aëronomie, Ringlaan 3, B-1180, Brussels, Belgium. (jan.dodion@bira-iasb.be)